ISBN: 978-3-95450-253-0 ISSN: 2673-5571 doi:10.18429/JACoW-HB2023-WEA2I1

COMPENSATION OF THIRD-ORDER RESONANCES IN THE HIGH-INTENSITY REGIME

C. E. Gonzalez-Ortiz*, P. N. Ostroumov[1], Michigan State University, East Lansing, MI, USA
R. Ainsworth, Fermilab, Batavia, IL, USA
[1] also at FRIB, East Lansing, MI, USA

Abstract

As the Fermilab Accelerator Complex enters the high-intensity era, the Recycler Ring (RR) needs to mitigate the detrimental effect of third-order resonance crossing. Third-order resonance lines can be compensated to first order by cancelling out the global Resonance Driving Terms (RDTs) using the response matrix method. This compensation scheme has been proven to work at low intensities, i.e., in the single-particle regime. In order to evaluate the effectiveness of this compensation scheme at higher intensities, this study looks at dynamic and static tune scans, with and without resonance compensation, and different space charge tune shifts.

INTRODUCTION

The Recycler Ring is a permanent-magnet storage ring located in the Fermilab Accelerator Complex. This machine stores bunched protons at a fixed energy of 8 GeV. It shares the same tunnel with the Main Injector (MI), both with a circumference of around 3.3 km (2.06 miles). For high-intensity operation, i.e., for beam delivery to the Neutrinos at Main Injector (NuMI) experiment, the RR slip-stacks protons coming from Booster and, ultimately doubles the intensity for the stored beam. Protons are then injected into MI, where they are accelerated to an energy of 120 GeV and sent to NuMI [1–3]. Table 1 summarizes the properties of typical beam in the RR that gets sent to NuMI.

The Proton Improvement Plan II (PIP-II) is the first step in establishing the Fermilab Accelerator Complex as a multi-MW proton facility [4]. The near-future objective is to deliver a 1.2 MW proton beam to the Deep Underground Neutrino Experiment (DUNE) through the Long-Baseline Neutrino Facility (LBNF). In order to meet this goal, several upgrades are being planned in the accelerator complex, including a new 800 MeV superconducting linear accelerator. With minimal upgrades to the Main Injector and Recycler Ring, but with a substantial overhaul of the Booster Ring, this will allow for a 50 % increase in particles per pulse intensity. Table 1 also specifies some upgrades that will happen for the PIP-II era. Some examples include an increase of the particle per bunch intensity, a shortening of the Main Injector acceleration ramp and an increase in the Booster ramping rate.

As the Recycler Ring starts to deal with higher intensities, it is important to mitigate the harmful effects of space charge. Specifically, this work focuses on the excitation of third-order betatron resonances due to the incoherent space charge detuning of particles in the beam. Particles in the core of the beam will experience a larger space charge force leading to detuning in their betatron frequencies. Given the incoherent nature of this process, this leads to the beam having a larger tune spread in the tune diagram. Figure 1 shows the tune footprint for particles with transverse amplitudes up to 3σ, assuming a Gaussian bunched beam. This detuning was calculated using PySCRDT [5, 6], but can also be estimated assuming a uniform bunched beam [7, 8]. Particles will also experience an additional tune shift due to uncorrected chromaticity and slip stacking operation [3].

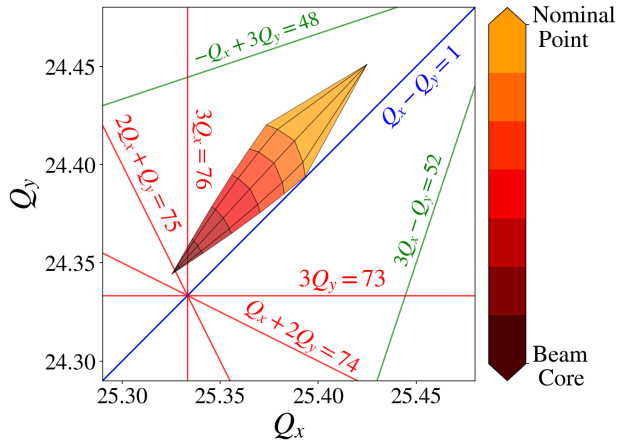

Figure 1: Space charge tune footprint calculated using PySCRDT [5] for 1×10^{11} particles per bunch in a PIP-II Recycler Ring.

Figure 1 shows how for typical operation to NuMI under future PIP-II specifications, there is a space charge tune shift of around 0.1 in both planes. At nominal tunes, it is clear that for high-intensity operation the particles in the core of the beam will start to operate on top of third-order resonances. These third-order resonances include two normal sextupole lines ($3Q_x = 76$ and $Q_x + 2Q_y = 74$) and two skew sextupole lines ($3Q_y = 73$ and $2Q_x + Q_y = 75$). It is also worth pointing out that the coupling line $Q_x - Q_y = 1$ is already being corrected for with skew quadrupoles. The following work, complemented with previous work in Refs. [9, 10], explores how cancelling out the global resonance driving terms (RDTs) of these resonance lines can mitigate their harmful effect in the low and high-intensity regime. Furthermore, this work outlines the challenges to overcome for complete implementation of the mitigation scheme for high-intensity operation at the Fermilab Recycler Ring.

* gonza839@msu.edu

ISBN: 978-3-95450-253-0 ISSN: 2673-5571 doi:10.18429/JACoW-HB2023-WEA2I1

Table 1: Recycler Ring properties for beam sent to NuMI

Parameter	Nominal Value	Unit
Circumference	3319	m
Momentum	8.835	GeV/c
RF Frequency	52.8	MHz
RF Voltage	80	kV
Harmonic Number	588	
Synchrotron Tune	0.0028	
Slip Factor	-8.6 10^{-3}	
Superperiodicity	2	
Horizontal Tune	25.43	
Vertical Tune	24.445	
Horizontal Chromaticity	-6	
Vertical Chromaticity	-7	
95% Normalized ϵ	15 π	mm mrad
95% Longitudinal ϵ	0.08	eV s
Particles / Bunch	5 10^{10}	
Particles / Bunch (PIP-II)	8 10^{10}	
MI Ramp Times	1.333	s
	1.133	s
	1.067	s
Booster Frequency	15	Hz
Booster Freq. (PIP-II)	20	Hz

COMPENSATION OF THIRD-ORDER RESONANCES AT LOW INTENSITIES

Betatron resonances in circular accelerators arise from multipole field perturbations found around the ring. These field perturbations can come from some systematic error in the magnets from each periodic cell, from a random error unrelated to the superperiodicity of the machine or from higher order multipoles introduced in the machine, i.e., sextupoles, octupoles or other higher order multipoles [11]. For the specific case of the Recycler Ring and its third-order resonances, the perturbation sources are the permanent magnets which are combined function magnets with substantial sextupole component. Additionally, there are sextupoles for chromaticity correction that can also drive these third-order resonances.

Global Third-order RDTs

The strength of each resonance line can be quantified using the global resonance driving terms (RDTs) expansion [12]. Assuming h is the Hamiltonian term that absorbs all the perturbations to the linear one turn map of a circular accelerator, one can expand h as:

$$h = \sum_{jklm} h_{jklm} \left(2J_x\right)^{\frac{j+k}{2}} \left(2J_y\right)^{\frac{l+m}{2}} e^{i\left[(j-k)\phi_x + (l-m)\phi_y\right]}, \tag{1}$$

where j, k, l and m are indices related to the four variables of transverse phase space, h_{jklm} are complex numbers called global resonance driving terms, and (J_x, ϕ_x) and (J_y, ϕ_y) are the two pairs of action angle-variables for linear uncoupled dynamics. The RDTs h_{jklm} can be traced to the resonance lines, given that the following condition must hold: $(j-k)Q_x + (l-m)Q_y = p$, where p is an integer. For third-order resonances in the Recycler, it is of interest to look at the third-order RDTs, i.e., $j+k+l+m = 3$. Table 2 shows the RDT to be measured for each third-order resonance line close to the operation point of the RR.

Table 2: Characterization of the third-order resonance lines close to Recycler Ring operation

Res. Line	RDT	Sext. Term
$3Q_x = 76$	h_{3000}	Normal
$Q_x + 2Q_y = 74$	h_{1020}	Normal
$3Q_y = 73$	h_{0030}	Skew
$2Q_x + Q_y = 75$	h_{2010}	Skew

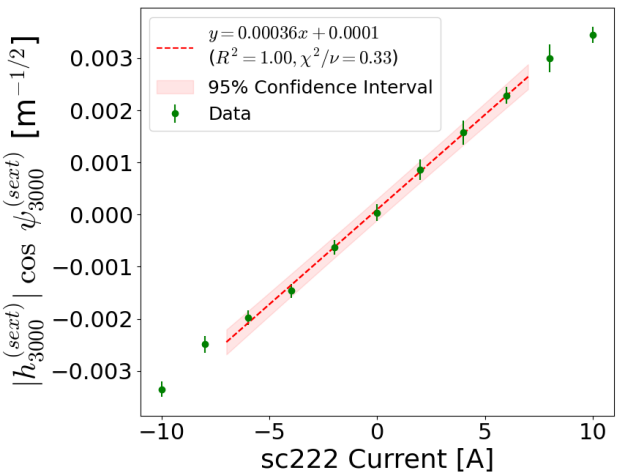

Figure 2: Real part of RDT against normal sextupole 222 current for a particular BPM.

Compensation Scheme

The compensation scheme explored in this work focuses on cancelling out the global RDTs for a single resonance line or for multiple resonance lines. This is done with the help of two pairs of normal sextupoles and two pairs of skew sextupoles that have been previously installed with the sole purpose of compensating these resonances. First of all, the bare machine h_{jklm} terms must be measured, i.e., compensation sextupoles off. References [9, 10] explain the measurement technique used in order to analyze the spectral decomposition of BPM data and extract the RDTs.

Once the bare machine h_{jklm} is measured, the compensation sextupoles are scanned and the individual sextupole contribution to the RDT can be estimated. Fig. 2 shows a plot of the real part of the individual sextupole contribution to the RDT as a function of the sextupole current. A similar plot can be built for the imaginary part of $h_{3000}^{(sext)}$. This procedure can be applied for all the compensation sextupoles and the response matrix of the RDTs to the currents in the compensation sextupoles can be

ISBN: 978-3-95450-253-0 ISSN: 2673-5571 doi:10.18429/JACoW-HB2023-WEA2I1

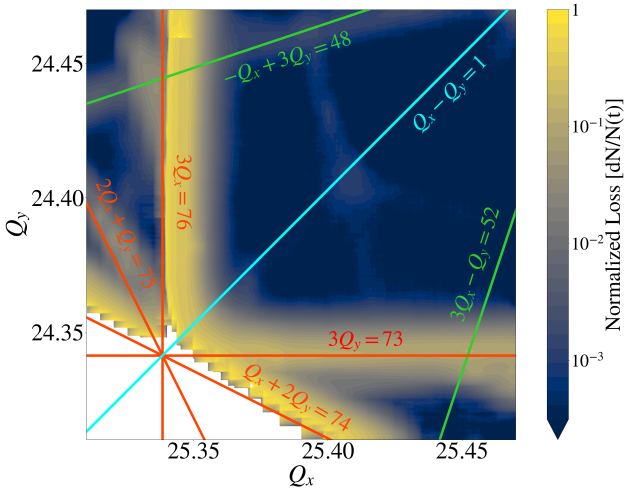

Figure 3: Dynamic loss map for the Recycler Ring with the closest resonance lines superimposed up to fourth order for around 1×10^{10} ppb.

calculated. Once the response matrix is calculated, it can be inverted in order to get the compensation currents that cancel out the h_{jklm} term, e.g., the currents in the compensation normal sextupoles that cancel out the h_{3000} term.

Dynamic Loss Maps

In order to verify compensation of the resonance lines, several methods can be applied. Nevertheless, the focus of this work will be using dynamic loss maps. Dynamic loss maps are created by mapping out the losses in a specific region of the tune diagram. In the Recycler Ring, these loss maps can be created by introducing tune ramps by means of the phase trombone program [13]. At least two scans (horizontal and vertical) are required to create the loss map shown in Fig. 3.

The first horizontal scan is created by holding the vertical tune constant, and putting a horizontal tune ramp that goes from $Q_x = 25.47$ to $Q_x = 25.31$. The *constant* vertical tune is then changed from $Q_y = 24.47$ to $Q_y = 24.31$ in steps of 0.005, while recording the intensity data. For the vertical scan, the roles are reversed. The horizontal tune is held constant, and a vertical tune ramp is introduced that goes from $Q_y = 24.47$ to $Q_y = 24.31$. The *constant* horizontal tune is then changed from $Q_x = 25.47$ to $Q_y = 25.31$ in steps of 0.005. The intensity data from both scans can be differentiated, normalized by the instantaneous intensity and interpolated in a two-dimensional grid in order to build plots such as the ones shown in Figs. 3 and 4.

Figure 3 shows how the loss patterns align with the theoretical location for the resonance lines. There is a slight shift in the set tune and the real tune due to the calibration from the tune trombone program. Nevertheless, the resonance line structure in the loss pattern allows for visualization of the strength of each resonance, i.e., the stronger the RDT for a resonance line is, the higher the normalized losses are in that particular tune location. Figure 3 shows third, fourth and even hints of fifth order resonance lines, with third-order resonance lines being the strongest.

Figure 4 shows dynamic loss maps for several configurations of the compensation sextupoles. Figure 4a shows the bare machine loss map, i.e., no compensation sextupole turned on, while Fig. 4b and Fig. 4c shows the compensation for a single resonance line. For the $3Q_x$ compensation, the four normal sextupoles are set to the compensation currents as calculated with the RDT response matrix method. It is worth clarifying that for Fig. 4b, there is an artificial loss line at $Q_y = 24.395$ due to a wrong configuration of the dampers while performing the experiment. Nevertheless, if Fig. 4b is compared to Fig. 4a, it is clear the normalized losses at the $3Q_x$ line decrease by two orders of magnitude with compensation. The same holds for the $3Q_y$ compensation in Fig. 4c.

Figures 4d, 4e and 4f show the optimum configurations of the compensation sextupoles that compensate multiple resonance lines. It is worth pointing out that for some of these configurations when trying to compensate one or multiple resonance lines, other resonance lines might become stronger. Such is the explicit case in Fig. 4f, where by compensating $3Q_y$ and Q_x+2Q_y, the resonance $2Q_x+Qy$ grows stronger. This is a limitation for trying to compensate more than two resonance lines, given that the compensation currents grow larger. There is a limit in the currents that are fed to the compensation sextupoles. For example, the currents needed to compensate both normal sextupole lines, $3Q_x$ and $Q_x + 2Q_y$, go over the current limit. There is ongoing effort to bring down the compensation currents for this particular case.

Another detail worth noting in Figs. 4a-4f is the white area in the loss maps which represents the regions for where there was not enough beam to map out the losses. For some particular configurations the compensation sextupoles, the combined strength of the third-order resonance lines decreases in such a way that there is still some beam left past the lines. An argument could be made that two additional scans can be made, injecting from the left and from the bottom, in order to map out these unavailable regions. This addition can be a future upgrade to these loss maps. Ultimately, all these plots in Fig. 4 show several possible configurations that free up regions of tune space to be used during operations in order to fit high-intensity beam.

COMPENSATION OF THIRD-ORDER RESONANCES AT HIGH INTENSITIES

The last section showed results for experiments done at low intensities, i.e., particle per bunch intensities of around 1×10^{10}. As table 1 specifies, PIP-II is going to operate at intensities of almost 1×10^{11} particles per bunch (ppb) – one order of magnitude higher. Therefore, it is of interest to characterize this compensation scheme at higher intensities. Specifically, for the Recycler Ring, the intensity can be varied by controlling the number of Booster turns injected.

ISBN: 978-3-95450-253-0 ISSN: 2673-5571 doi:10.18429/JACoW-HB2023-WEA2I1

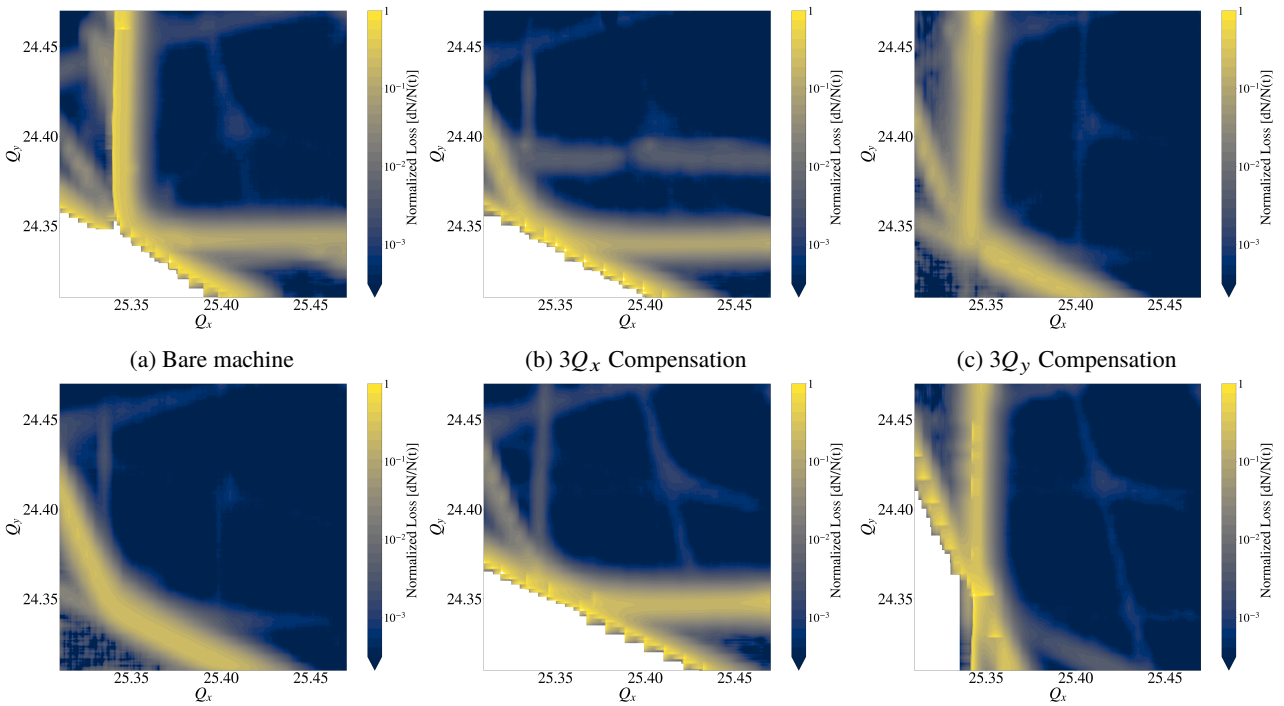

(a) Bare machine (b) $3Q_x$ Compensation (c) $3Q_y$ Compensation

(d) $3Q_x$ and $3Q_y$ Compensation (e) $3Q_x$ and $2Q_x + Q_y$ Compensation (f) $3Q_y$ and $Q_x + 2Q_y$ Compensation

Figure 4: Dynamic loss maps for several configurations of compensation sextupoles

Experiments at low intensities are done at 2 Booster turns (BTs) equivalent to approximately 0.7×10^{10} ppb.

Dynamic Loss Maps

Dynamic loss maps are measurements that depend on the characteristics of the beam used. When trying to create the loss maps with high-intensity beam, special care has to be taken in order to address the space charge tune shift. An analogy can be made between drawing a painting with a thin or a thick brush and creating loss maps with a low intensity or high-intensity beam.

Dynamic loss maps in the Recycler Ring have been created at 12 Booster turns (BTs), approximately 4.4×10^{10} ppb. Nevertheless, the result was a blur of losses all around the tune space, given that the incoherent space charge tune shift was too large to resolve the resonance lines individually. Nevertheless, slices of high-intensity loss maps can be used to measure the space charge tune spread.

Figure 5 shows slices of loss maps at different intensities. The top slice corresponds to an intensity of 2 BTs, i.e., approximately 0.6×10^{10} ppb. The bottom slice corresponds to an intensity of 17 BTs, approximately 6.0×10^{10} ppb, which is close to the maximum intensity that can be provided by Booster in single batch. The important thing to note here is that as the intensity increases the losses happen early in the tune ramp. This can be correlated to the space charge tune spread using the location of the $3Q_x$ line, which corresponds to where all the beam is lost. For example, for the bottom slice the losses start happening at $Q_x = 25.37$, while all beam is lost at $Q_x = 25.345$. This means the space charge tune spread can be approximated to 0.025. Ultimately, Fig. 5 shows beams with space charge tune shifts that range from 0.005 to 0.025.

Another thing to note from Fig. 5 is how the space charge tune shift tends to stabilize to a value of around 0.025 for intensities higher than 12 BTs or 4.4×10^{10}. This is due to the fact that the equilibrium emittance grows exponentially at higher intensities. Specifically, Ref. [14] shows how the beam emittance grows with intensity in the Recycler Ring. This study combined with calculations of the space charge tune shift provided in Ref. [7], explain this behaviour. The emittance grows at the same pace as the beam intensity leading to a stable tune shift.

The maximum tune spread shown in Fig. 5 is around 0.025, which only compares to 1/4 of the PIP-II projection. It is worth pointing out, that these experiments are done for a single batch with no slip stacking. Therefore, with slip stacking and smaller beam emittance coming from Booster, space charge tune shifts in the RR of around 0.1 will be possible in the PIP-II era.

Static Tune Scans

One alternative to dynamic loss maps are static tune scans. This experimental technique involves fixing a particular set of tunes and measuring how much beam survives compared to how much beam was injected, i.e., the beam survival ratio. This ratio can help characterize the effectiveness of the resonance compensation scheme at higher intensities. The following experiments were done by measuring the

ISBN: 978-3-95450-253-0 ISSN: 2673-5571 doi:10.18429/JACoW-HB2023-WEA2I1

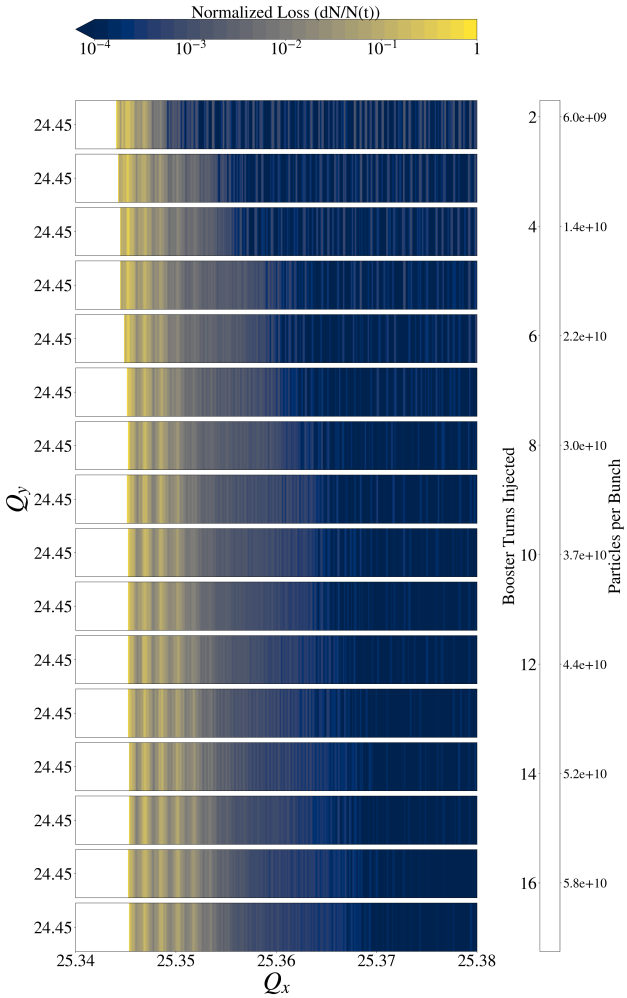

Figure 5: Dynamic loss map slice close to the $3Q_x$ resonance for a fixed vertical tune of $Q_y = 24.44$ at different intensities.

beam survival ratio for a single batch in the Recycler after 0.8 seconds, i.e., around 70000 turns.

Figure 6 shows two static tune scans, one for the bare machine (left plot) and one with the h_{3000} term cancelled (right plot) at low intensity, i.e., 2 BTs equivalent to 0.71×10^{10} ppb. The left-pointing arrows in the plot are meant to illustrate the space charge tune spread as measured in the last section. These scans cross $3Q_x = 76$ and the fourth order line $-Q_x + 3Q_y = 48$ at a vertical tune of $Q_y = 24.44$. For the left plot of Fig. 6, the big dip in beam survival ratio happening at around $Q_x = 25.34$ corresponds the $3Q_x$ resonance, while the dip at around $Q_x = 25.325$ corresponds to the fourth order resonance line. The vertical band highlighted in red corresponds to the region where no beam survives at this intensity. This band is used as reference for the other scans shown in Figs. 6, 7 and 8.

The right plot of Fig. 6 shows a static tune scan with the optimum configuration in the compensation sextupoles that cancels out the h_{3000} term. For beam on top of the red band, beam now survives almost with a ratio of 1, whereas in the left plot no beam would survive at this region. The

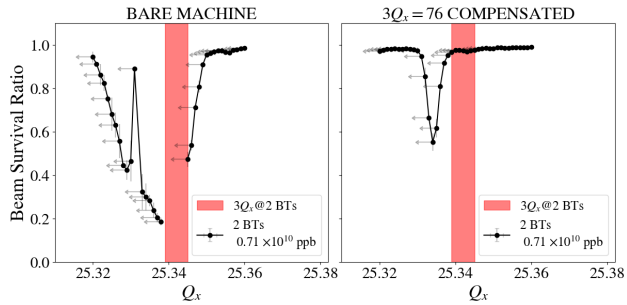

Figure 6: Static tune scan with and without $3Q_x$ compensation for an intensity of 2 Booster Turns or approximately 0.71×10^{10} ppb. Measurements were done at $Q_y = 24.44$.

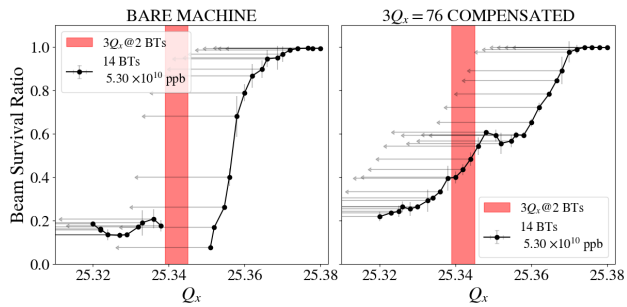

Figure 7: Static tune scan with and without $3Q_x$ compensation for an intensity of 14 Booster Turns or approximately 5.2×10^{10} ppb. Measurements were done at $Q_y = 24.44$.

dip from the fourth order resonance can still be seen and is now shifted a small amount to the right. Nevertheless, these static tune scans prove that the third-order resonance is being compensated to an acceptable degree at low intensities.

Figure 7 shows a static tune scan for an intensity of 14 Booster turns equivalent to 5.30×10^{10} and resulting in a space charge tune shift of around 0.025. The experimental setup for these scans are the same as the ones shown in Fig. 6, just at a higher intensity. The first thing to note is that for the left plot, the one with no compensation, the beam starts to fall of earlier compared to the left plot of Fig. 6. This is due to the fact that space charge tune shift is larger for these measurements, as illustrated with the left-pointing arrows in the plot. Even though the beam is set to a nominal tune away from the resonance line, there are still particles that feel a detuning due to space charge and oscillate at a tune closer to the $3Q_x$ line.

The right plot of Fig. 7 shows the compensated case. Where as no beam would survive on top of the red band for the left plot, this compensated scan shows that beam can now survive in this region. Nevertheless, the improvement is not as significant as in the low intensity case, given that the beam survival ratio isn't close to 1. For this high-intensity measurement, the space charge tune spread is large enough that different particles in the bunch might be operating on top of different resonance lines at the same time.

ISBN: 978-3-95450-253-0 ISSN: 2673-5571 doi:10.18429/JACoW-HB2023-WEA2I1

Nevertheless, the fact that the beam survival ratio increases at high intensities with compensation on is encouraging. This means that the compensation scheme is beneficial, not only at low intensities but also at high intensities. Nevertheless, for high-intensity operation there are still other factors to be taken into account, as will be explored in the next section. One of those are the transverse dampers. For the experiments shown in Figs. 6 and 7, it is worth pointing out that these dampers were turned on.

High-Intensity Operation

The ultimate objective of this work is to have this resonance compensation scheme fully characterized in order to incorporate it into high-intensity operations. Nevertheless, there are two additional factors that have been identified to also play a role in this effort. The first one stems from the fact that the Main Injector and the Recycler Ring share the same tunnel. It has been shown that the acceleration ramp changes the beam dynamics inside the Recycler Ring. In particular, it introduces orbit distortions and tune shifts depending on the position of the ramp [15]. There is an ongoing effort in order to characterize any higher order magnetic effect from the MI to RR, e.g., any sextupole term that is being introduced by the MI acceleration ramp. The first results have shown that the compensation currents change depending on the location of the study event with respect to the MI acceleration ramp. Therefore, in the future, the resonance compensation described hereinabove should be modified to accommodate this effect to be fully operational.

The second factor is the use of transverse dampers to stabilize high-intensity operation. These dampers are used to control resistive wall instabilities in the Recycler Ring [1]. Figure 8 shows two static tune scans across the $3Q_x$ resonance, both with compensation on, but one with dampers on (left plot) and one with dampers off (right plot). It is worth pointing out, that the beam used to build Fig. 8 plots is different from the one used in Figs. 6 and 7. For this particular experiment, beam was injected close to the intersection of the third-order resonance lines, in order to have a controlled beam blowup without any losses. A thicker beam decreases the incoherent space charge tune shift [7]. After the emittance of the beam is blown up, a tune ramp is introduced to the locations specified by the static tune scan.

The left plot of Fig. 8 shows the beam survival ratio as a function of horizontal tune with $3Q_x$ compensation and dampers on. There is a big dip at the location of the $3Q_x$ resonance, even with the optimum configuration of compensation sextupoles. The right plot of Fig. 8 shows the result of turning off the dampers for this experiment. There is a clear increase in the beam survival ratio on top of the resonance. This suggests two things. The damper configurations for this experiment were not tuned for operation close to the $3Q_x$ resonance. And the dampers can excite this third-order resonance even with the compensation scheme in place. Further investigation is being conducted into this subject.

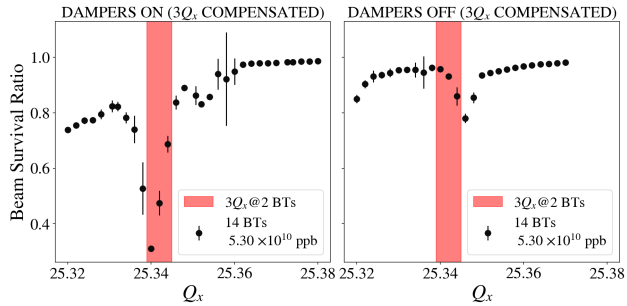

Figure 8: Static tune scan for thick beam close to the $3Q_x$ resonance for bare machine with dampers on (left), with $3Q_x$ compensation/dampers on configuration (center), and with $3Q_x$ compensation/dampers off configuration (right). Measurements were done at $Q_y = 24.43$.

CONCLUSION

Cancellation of global third-order RDTs allows to mitigate the harmful effect of third-order resonances in the Recycler Ring. This mitigation scheme reduces losses in the tune space regions, allowing for more beam to operate and survive close to these resonance lines. At higher intensities, this compensation scheme is also beneficial to the beam survival ratio. Nevertheless, the incoherent space charge tune shift complicates things when trying to use beam-based measurements, such as the ones used in this work. Further investigation is needed as to how the transverse dampers in the RR excite betatron resonances at high intensities.

ACKNOWLEDGMENTS

This manuscript has been authored by Fermi Research Alliance, LLC under Contract No. DE-AC02-07CH11359 with the U.S. Department of Energy, Office of Science, Office of High Energy Physics. We would like to acknowledge the ASET (Accelerator Science and Engineering Traineeship) program at Michigan State University. The ASET program is partially supported by the US Department of Energy, Office of Science, High Energy Physics under Cooperative Agreement award number DE-SC0018362 and Michigan State University.

REFERENCES

[1] R. Ainsworth *et al.*, "High-intensity operation using proton stacking in the Fermilab Recycler to deliver 700 kW of 120 GeV proton beam", *Phys. Rev. Accel. Beams*, vol. 23, no. 12, p. 121002, Dec. 2020. doi:10.1103/PhysRevAccelBeams.23.121002

[2] R. Ainsworth *et al.*, "Improvements to the Recycler/Main injector to deliver 850 kW+", in *Proc. NAPAC'22*, Albuquerque, NM, USA, Aug. 2022, pp. 578–580. doi:10.18429/JACoW-NAPAC2022-WEYE3

[3] R. Ainsworth *et al.*, "High-intensity space charge effects on slip stacked beam in the Fermilab Recycler", *Phys. Rev. Accel. Beams*, vol. 22, no. 2, p. 020404, Feb. 2019. doi:10.1103/PhysRevAccelBeams.22.020404

ISBN: 978-3-95450-253-0 ISSN: 2673-5571 doi:10.18429/JACoW-HB2023-WEA2I1

[4] M. Ball *et al.*, "The PIP-II conceptual design report", Fermilab, Batavia, IL, USA, Mar. 2017, Rep. FERMILAB-TM-2649-AD-APC1516858. doi:10.2172/1346823

[5] F. Asvesta, *et al.*, PySCRDT Repository. https://github.com/fasvesta/PySCRDT

[6] F. Asvesta, H. Bartosik, "Resonance driving terms from space charge potential"CERN, Geneva, Switzerland, 2019, Rep. CERN-ACC-NOTE-2019-0046. https://cds.cern.ch/record/2696190/files/CERN-ACC-NOTE-2019-0046.pdf

[7] S.Y. Zhang, T. Roser and W.T. Weng, "Calculation of incoherent space charge tune spread", Brookhaven National Lab., Upton, NY, USA, 1996, Rep. AGS/AD/Tech. Note No. 449. https://technotes.bnl.gov/PDF?publicationId=30778.

[8] O. Mohsen, R. Ainsworth, and N. Eddy, "Waker Experiments at Fermilab Recycler Ring", in *Proc. NAPAC'22*, Albuquerque, NM, USA, Aug. 2022, pp. 124–127. doi:10.18429/JACoW-NAPAC2022-MOPA33

[9] C.E. Gonzalez-Ortiz *et al.*, "Third-order resonance compensation at the FNAL Recycler ring", in *Proc. IPAC'22*, Bangkok, Thailand, Jun. 2022, pp. 195–198, doi:10.18429/JACoW-IPAC2022-MOPOST050

[10] C.E. Gonzalez-Ortiz *et al.*, "Simultaneous Compensation of Third-Order Resonances at the FNAL Recycler Ring", in *Proc. IPAC'23*, Venice, Italy, Jun. 2023, pp. 3328–3331, doi:10.18429/JACoW-IPAC2023-WEPL112

[11] H. Wiedemann "Resonances"in *Particle Accelerator Physics* Springer Cham., Stanford, CA, USA, July 2015, pp. 539–564. doi:10.1007/978-3-319-18317-6_16

[12] R. Bartolini and F. Schmidt, "Normal form via tracking or beam data", *Part. Accel.*, vol. 59, pp. 93–106, Aug. 1997, https://cds.cern.ch/record/333077

[13] M. Xiao, "Phase Trombone Program Migration for the Recycler Ring at Fermilab", in *Proceedings of the 2005 Particle Accelerator Conference*, Knoxville, TN, USA, 2005, pp. 3135–3137. doi:10.1109/PAC.2005.1591389.

[14] B. Babacan *et al.*, "The ionization profile monitors in the Recycler ring"in *Proc. IPAC'23*, Venice, Italy, Jun. 2023, pp. 4669–4672. doi:10.18429/JACoW-IPAC2023-THPL093

[15] N. Chelidze, R. Ainsworth, and K. J. Hazelwood, "The Effect of the Main Injector Ramp on the Recycler", in *Proc. NAPAC'22*, Albuquerque, NM, USA, Aug. 2022, pp. 90–92. doi:10.18429/JACoW-NAPAC2022-MOPA19